AIAA JOURNAL
Vol. 44, No. 11, November 2006

Tiltrotor Whirl Flutter Alleviation Using Actively Controlled Wing Flaperons

Eric L. Hathaway*
The Boeing Company, Philadelphia, Pennsylvania, 19142-0858
and
Farhan Gandhi†
Pennsylvania State University, University Park, Pennsylvania, 16802

DOI: 10.2514/1.18428

The present study is an evaluation of the effectiveness of wing flaperon active control for alleviation of tiltrotor whirl flutter. Control systems that increase whirl flutter speed and wing mode subcritical damping are designed while at the same time observing realistic limits on flaperon deflection. Both stiff- and soft in-plane tiltrotor configurations are examined, to develop an understanding of the influence of vehicle configuration on flaperon effectiveness. The importance of considering unsteady aerodynamic effects in stability analyses and in controller design is also discussed. Controller designs considered include gain-scheduled full-state feedback optimal control, constant-gain full-state controllers derived from the optimal controllers, and single-state feedback systems. The dominant feedback parameters in the optimal control systems are identified and examined to gain insight into the most important feedback paths that could be exploited by simpler reduced-order controllers. Feedback of wing vertical and chordwise bending modes are identified as the most powerful parameters, with wing vertical bending rate feedback being particularly beneficial, as it substantially increases wing vertical bending mode damping.

Introduction

TILTROTOR whirl flutter instability has been the focus of considerable analytical and experimental research. The fundamental cause of the instability, destabilizing in-plane hub forces generated by the airloads required to precess the rotor, has been well understood for some time. The conventional approach to ensuring adequate whirl flutter stability margins has required wing structures with very high torsional stiffness. This stiffness requirement leads to rather thick wing sections with associated high levels of aerodynamic drag, reducing the aircraft's range and its efficiency. While passive design techniques can improve tiltrotor aeroelastic stability, there may be limits to this approach, particularly in the case of soft in-plane rotor configurations, which are being considered for future tiltrotor designs. For instance, [1] reported that for soft in-plane tiltrotors, combinations of aeroelastic couplings that alleviate air resonance may be detrimental to whirl flutter stability. Furthermore, the few soft in-plane configurations that have been tested in a wind tunnel (see [2,3]) have exhibited unacceptably low levels of wing vertical bending mode damping even before the onset of whirl flutter. The marginal damping in this mode must be improved before these configurations can be used on production tiltrotors.

Another option for improving tiltrotor aeroelastic stability is the use of active controls. There have been several studies investigating the use of active controls on tiltrotor aircraft. Active control has been considered for purposes of gust alleviation [4], reduction of blade loads [5], and vibration reduction [6,7], as well as aeroelastic and aeromechanical stability augmentation [8–11].

During a test of the Boeing Model 222 soft in-plane rotor in the NASA Ames 40- by 80-foot wind tunnel, a simple feedback control system to increase damping of the poorly damped wing vertical bending mode was investigated [2]. An accelerometer mounted on the wingtip sensed vertical bending motion of the wing. Active control inputs to the system were introduced through the swashplate. After an open loop study to determine the best control gain and phase for the controller, closed loop tests were conducted. The controller was very successful at adding damping to the wing vertical bending mode.

In [4], Johnson analytically investigated the use of an optimal controller with an estimator for reduction of tiltrotor gust response for both the Boeing Model 222 and Bell XV-15 full-scale rotors tested at NASA Ames in the early 1970s. The actuation strategies considered included active wing flaperons and swashplate inputs, and a combination of the two. Both wing flaperons and swashplate-based controllers were effective at improving proprotor gust response. Because the lowly damped wing modes were an important part of the gust response, the controller acted to greatly increase the damping of the wing modes to reduce the response. Thus, although [4] did not explicitly consider the problem of aeroelastic instability, it did confirm that active control was a feasible technique for tiltrotor damping augmentation.

Studies by Nasu [8] and van Aken [9,10] analytically demonstrated the ability of a simple feedback control system using swashplate actuation to influence whirl flutter stability. No attempt was made in these studies to optimize the performance of the active control system. In [11], Vorwald and Chopra used optimal control techniques to improve whirl flutter stability. An LQR optimal controller with observer commanding inputs through the swashplate was formulated. A significant increase in predicted flutter speed was obtained, but no consideration was given as to whether the control inputs commanded by the controller were within physically realistic limits.

Active control of a wing flaperon for vibration reduction was experimentally examined in [6]. In this study, an active control system known as the multipoint adaptive vibration suppression system (MAVSS), designed by Bell Helicopters, was used to reduce 1P and 3P vibrations on the wing and rotor aeroelastic testing system (WRATS), a 1:5-scale semispan wind tunnel model based on the V-22. Wing strain gauges and accelerometers installed in the engine nacelle measured system response. In [7], the wing flaperon was used in conjunction with higher harmonic control swashplate inputs. With simultaneous swashplate and flaperon actuation, load reductions of 85 to 95% were achieved in all three wing modes.

Received 27 June 2005; revision received 22 December 2005; accepted for publication 10 January 2006.

*Engineer, Member AIAA.
†Professor, Rotorcraft Center of Excellence, Department of Aerospace Engineering. Senior Member AIAA.

More recently, a great deal of experimental work [3,12–14] has been performed at NASA Langley Research Center and Bell Helicopters to evaluate the effectiveness of a modern adaptive control algorithm known as generalized predictive control (GPC) for tiltrotor stability augmentation and vibration suppression. GPC is a digital time-domain multi-input, multi-output predictive control method [15]. System identification and control input calculations are performed online. The active control inputs are made through the swashplate. These experimental investigations have demonstrated the potential of a GPC-based controller to improve tiltrotor aeroelastic and aeromechanical stability. Complex adaptive control algorithms such as GPC, however, are not attractive for use in production aircraft due to the high cost of developing and certifying such a system.

Active control appears to have great potential to improve tiltrotor aeroelastic stability. Soft in-plane tiltrotors in particular appear to be prime candidates for the application of active stability augmentation systems, due to inherently poor damping of the wing vertical bending mode. Active control has recently been demonstrated experimentally on soft in-plane tiltrotors [3], but as of yet very few analytical studies of active control for soft in-plane tiltrotor stability augmentation have appeared in the literature. Previous studies investigating tiltrotor active stability augmentation have largely focused on active control using inputs through the swashplate. Little attention has been paid to active control of a wing flaperon for tiltrotor aeroelastic stability augmentation. An actively controlled wing flap should be effective for increasing tiltrotor whirl flutter stability boundaries, due to the large control authority of the aerodynamic surface in high speed cruise.

The active control strategies considered in previous studies varied considerably in terms of sophistication of the controller, from simple unoptimized feedback controllers that served to demonstrate the feasibility of active control, to complex adaptive control systems. A full-state optimal controller would provide a useful benchmark for analytical investigations of tiltrotor active control, as the performance of such a controller would establish the maximum possible stability augmentation for a given system. It should be noted that the performance of the GPC controllers used in the NASA Langley studies approach that of an optimal controller as the prediction horizon of the predictive controller is increased. Thus, the relatively simple optimal controller can also indicate the maximum performance potential of the more complex adaptive controller.

The focus of the present study is to evaluate the effectiveness of wing flaperon active control for alleviation of whirl flutter. The study seeks to establish how large an increase in flutter speed may be achieved while at the same time observing realistic limits on flaperon deflection. Both stiff- and soft in-plane tiltrotor configurations are examined, to develop an understanding of the influence of vehicle configuration on flaperon effectiveness. The importance of considering unsteady aerodynamic effects in stability analyses and in controller design is also examined. The study focuses on optimal control systems using full-state feedback. Feedback gains from the optimal controllers are examined to gain insight into the most important feedback paths that could be exploited by simpler reduced-order controllers.

Analytical Model

Overview of Analytical Model

The analytical model used in the present investigation was developed in [16], and was used in [17] to perform passive design optimization studies to improve tiltrotor whirl flutter stability. The model represents a proprotor with three or more blades, mounted on a semispan, cantilevered wing structure. The wing is modeled using the finite element method as an elastic beam undergoing vertical bending, chordwise bending, and elastic torsion. The nacelle is modeled as a mass rigidly attached to the wingtip. Offsets of the nacelle center of mass from the wingtip elastic axis are included. Modal reduction of the FEM wing/nacelle model is performed to reduce the total number of system degrees of freedom. The first three wing modes—vertical bending (b), chordwise bending (c), and torsion (t)—are retained in this study.

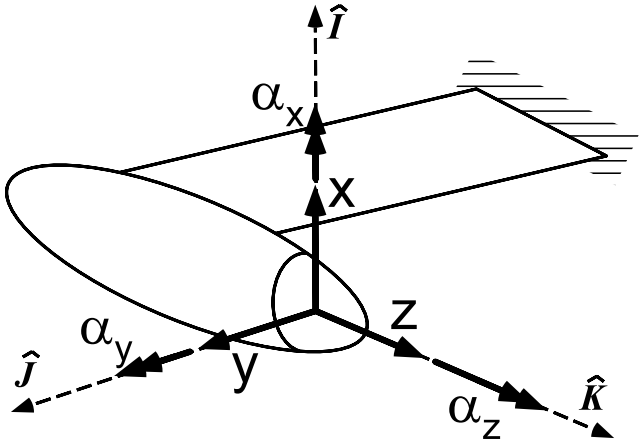

Fig. 1 Rotor hub degrees of freedom.

The rotor hub experiences both displacements (x, y, z) and rotations $(\alpha_x, \alpha_y, \alpha_z)$ in space, as shown in Fig. 1. The hub may be gimballed, allowing cyclic flapping motion at the blade root (β_G). In the fixed frame, this gimbal degree of freedom allows for longitudinal (β_{GC}) and lateral (β_{GS}) tilting of the rotor disk. The blade is attached to the hub with some precone angle β_P. Perturbation of rotor azimuthal position in the rotating frame (ψ_s) is included, allowing a windmilling rotor condition to be modeled. Blade flapping motion (β) and in-plane lead-lag motion (ζ) are also included. Figures 2 and 3 illustrate the blade out-of-plane and in-plane degrees of freedom. Rotor aerodynamics are calculated using quasisteady blade element theory, with corrections applied to the

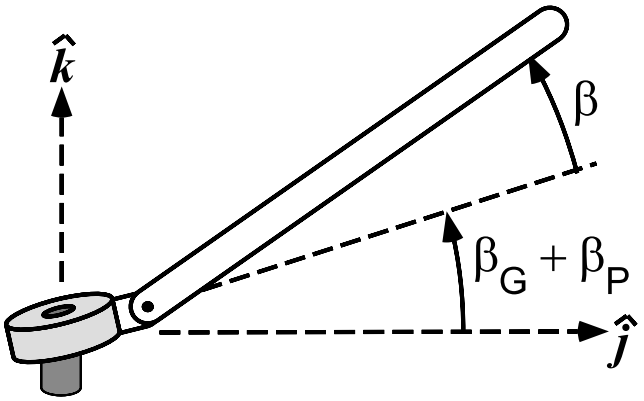

Fig. 2 Gimbal and blade flapping degrees of freedom.

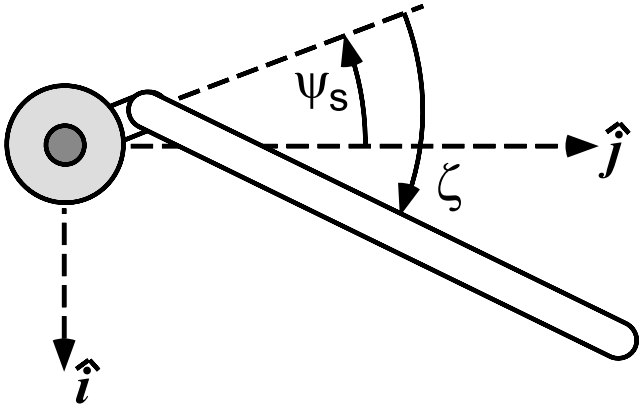

Fig. 3 Rotor azimuthal position and blade lead-lag degrees of freedom.

blade lift and drag coefficients to account for compressibility effects. The model of blade stiffness associated with flap and lag motion allows for blade flexibility to be distributed inboard and outboard of the pitch bearing. By allowing blade flexibility outboard of the pitch bearing, the analysis can directly model the variations in rotor frequencies and pitch-flap and pitch-lag couplings that occur with changes in collective pitch. Other rigid-blade tiltrotor stability analyses typically rely upon tabulated input data to represent these variations in rotor frequency and couplings.

The rotor degrees of freedom are transformed to the nonrotating frame using a multiblade coordinate transformation. To couple the rotor to the wing/nacelle system, the rotor hub degrees of freedom are transformed into the wing modal degrees of freedom. The work done on the wing by the rotor is expressed in terms of the hub forces and moments and added to the wing equations of motion, resulting in a set of fully coupled rotor/wing equations.

See [16] for an in-depth description of the unique features of the present model, and a discussion of the impact of these modeling features on whirl flutter stability prediction. Extensive validation results, comparing the present analysis to existing elastic blade tiltrotor stability analyses and to experimental test data for several different tiltrotor configurations, may also be found in [16].

Flaperon Active Control Formulation

Active control inputs to the system are through wing flaperon deflection (δ). In the present study, the flaperon is sized to approximately match the XV-15's flaperon, with a chord equal to 25% of the total wing chord, and a span covering the outer 50% of the wing. Aerodynamic forces and moments generated by flaperon motion are in general functions of flaperon displacement, rate, and acceleration. Thus the rotor/wing equations of motion, including the forcing terms due to flaperon motion, may be written as

$$[M]\overset{\star\star}{\boldsymbol{q}} + [C]\overset{\star}{\boldsymbol{q}} + [K]\boldsymbol{q} = [D_2]\overset{\star\star}{\delta} + [D_1]\overset{\star}{\delta} + [D_0]\delta \tag{1}$$

where $\boldsymbol{q}$ is the vector of wing and rotor degrees of freedom and $[M]$, $[C]$, and $[K]$ are the rotor/wing mass, damping, and stiffness matrices. These matrices contain both aerodynamic and structural contributions, the details of which are given in [16]. The matrices $[D_2]$, $[D_1]$, and $[D_0]$ relate the forces generated by the flaperon to flaperon acceleration, rate, and displacement, respectively. These matrices may include contributions due to flap inertial effects, as well as aerodynamic terms. In the absence of inertial terms, the matrix $[D_2]$ is zero for a simple quasisteady aerodynamic model, but is nonzero when unsteady aerodynamic effects are included. A quasisteady aerodynamic model will still contain forces proportional to flap rate $[D_1]$, as well as displacement $[D_0]$. For instance, if the flap aerodynamic model were based upon a quasisteady simplification of Theodorsen's unsteady aerodynamic model [18], the contribution to airfoil section lift from the flap would be

$$\Delta l = \frac{1}{2}\rho V^2 c\left(2T_{10}\delta + \frac{c}{2V}T_{11}\dot{\delta}\right) \tag{2}$$

where T_{10} and T_{11} are simply geometric constants related to the ratio of flap chord length to overall airfoil chord length, and are defined by Theodorsen in [18]. An aerodynamic model that also includes unsteady effects would have additional terms proportional to flap displacement, rate, and acceleration.

For control system design and analysis, it is convenient to express the system in the familiar first-order form $\dot{x} = Ax + Bu$. If forces and moments proportional to flaperon rate and acceleration were to be neglected, the system could easily be placed in such a form, using flaperon deflection δ as the control variable u. A more rigorous approach, which retains the aerodynamic loads proportional to flaperon rate and acceleration, is used in the present study. The control variable used is the flaperon acceleration:

$$u = \overset{\star\star}{\delta} \tag{3}$$

By formulating the control system to prescribe flaperon acceleration, and including flaperon angular displacement and rate in an augmented state vector (along with the wing and rotor degrees of freedom), the complete system can be expressed in the desired first-order form

$$\begin{Bmatrix} \overset{\star\star}{\boldsymbol{q}} \\ \overset{\star\star}{\delta} \\ \overset{\star}{\boldsymbol{q}} \\ \overset{\star}{\delta} \end{Bmatrix} = \begin{bmatrix} -M^{-1}C & M^{-1}D_1 & -M^{-1}K & M^{-1}D_0 \\ 0 & 0 & 0 & 0 \\ I & 0 & 0 & 0 \\ 0 & 1 & 0 & 0 \end{bmatrix} \begin{Bmatrix} \overset{\star}{\boldsymbol{q}} \\ \overset{\star}{\delta} \\ \boldsymbol{q} \\ \delta \end{Bmatrix} + \begin{bmatrix} M^{-1}D_2 \\ 1 \\ 0 \\ 0 \end{bmatrix} \overset{\star\star}{\delta} \tag{4}$$

Flaperon acceleration is determined by the feedback control law

$$\overset{\star\star}{\delta} = -[G]\begin{Bmatrix} \overset{\star}{\boldsymbol{q}} \\ \overset{\star}{\delta} \\ \boldsymbol{q} \\ \delta \end{Bmatrix} \tag{5}$$

where $[G]$ is the set of control gains to be determined by the controller design process.

Incorporation of unsteady aerodynamic forces will add additional terms and states to the system in Eq. (4). Formulation of the model including unsteady effects is discussed briefly in a later section and in greater detail in [19].

Limits on Control Gains

An important issue when evaluating the effectiveness of an active control scheme is the question of control gain limits. A given set of controller gains may be able to completely eliminate whirl flutter, but if the resulting control inputs command flap motions that greatly exceed the practical limits of flap deflection, the design is not feasible. To obtain an approximate estimate of control gain limits for the results presented here, some assumptions are made about maximum allowable flap deflection and about the magnitude of perturbations experienced by the wing modes. Flap deflection available to the active controller is assumed to be ± 6 deg. The 6 deg limit on flap deflection was selected based on practical considerations of aircraft control and actuator capability. In [20], the limits on flaperon deflection for the XV-15 operating in airplane mode are given as ± 15 deg. In [6], active control of the flaperon on the WRATS semispan model was examined experimentally for vibration suppression. In that test, the flaperon was driven up to ± 4 deg of deflection, but at a higher frequency (3/rev) than is required for stability augmentation. Therefore 6 deg was selected as an aggressive but not unrealistic target for maximum flap deflection for this study.

Another important parameter in determining limits on control gains is the level of perturbation experienced by the system. In a linear feedback control system of the form $u = -Gx$, for a fixed maximum control input u, the magnitude of controller gains G for which the controller input does not exceed prescribed limits are reduced as the level of disturbance x is increased. For an actual control design intended for practical implementation, a worst-case disturbance condition must be identified, and controller gains limited to prevent the control input from exceeding the prescribed limits, even for these worst-case conditions. As an approximation, the following perturbations are considered for the semispan tiltrotor model as the critical conditions used to limit controller gains: 1) wing vertical bending mode excitation, with wingtip vertical displacement of 2.5% of the rotor radius, 2) wing chordwise bending mode excitation, with a wingtip displacement of 1% rotor radius in the chordwise direction, and 3) wing torsion mode excitation, with 1 deg of twist at the wingtip. The controller gains used in the present study are chosen such that, given any one of the above disturbance

conditions, the resulting flap deflections will not exceed the maximum ±6 deg limit.

While the assumed disturbance conditions used in the present study could be considered somewhat artificial (excitation of a single mode to a known maximum level of perturbation), it should be noted that these disturbance conditions closely resemble the excitations typically applied to tiltrotor models undergoing aeroelastic testing in a wind tunnel. Piatak et al. [21] describes how the WRATS semispan tiltrotor model is excited during whirl flutter testing through "stick stirs," oscillatory blade pitch changes introduced through the swashplate at a wing mode natural frequency. The stick stir continues until a sufficient excitation amplitude of the wing mode is achieved, whereupon the excitation is removed, and the free response of the model is measured to obtain modal frequency and damping data. If the active flaperon control laws developed in the present study were implemented on a model undergoing similar testing, the limits imposed on controller gains would ensure that typical test excitations would not result in excessive flaperon commanded deflections.

Wing Unsteady Aerodynamic Modeling

In the initial model formulation, the wing aerodynamics were based on a quasisteady aerodynamic model. Because the actively controlled flaperon is capable of generating large oscillatory aerodynamic loads on the wing, the appropriateness of this simple aerodynamic model should be investigated. To this end, an unsteady aerodynamic model was added to the wing. By comparing the results obtained using each of these models, the influence of unsteady aerodynamics on performance of the actively controlled flaperon and on controller design can be evaluated to determine whether or not the quasisteady aerodynamic model is adequate. This section describes the general approach used to incorporate an unsteady aerodynamic model for the wing and flaperon in the present analysis. Hathaway [19] provides more specific implementation details.

To incorporate unsteady aerodynamics into the present tiltrotor wing model in a manner amenable to stability analysis and controller design, the aerodynamic model must be formulated in the time domain. A rational function approximation (RFA) approach is used in the present study to generate a state-space, time-domain aerodynamic model from oscillatory response data (airfoil lift and pitching moment about the quarter-chord and moments about the flap hinge, due to airfoil pitching and plunging and flap motions). The RFA technique has been commonly used in fixed-wing aeroelastic analysis. In [22], an RFA aerodynamic model was extended to account for unsteady freestream and Mach number effects and was successfully applied to a helicopter rotor with trailing-edge flaps. The RFA aerodynamic model used in the present study generally follows the formulation given in [22]. A brief description of the present formulation is provided below.

Consider the aerodynamic loads on an airfoil section, expressed in the Laplace domain:

$$\boldsymbol{F}(\bar{s}) = \boldsymbol{Q}(\bar{s})\boldsymbol{H}(\bar{s}) \tag{6}$$

where $\boldsymbol{F}(\bar{s})$ is a vector of generalized loads (in this case, sectional lift, pitching moment, and hinge moment), $\boldsymbol{H}(\bar{s})$ is a vector of generalized motions (due to pitch, plunge, and flap deflection and rate), and $\boldsymbol{Q}(\bar{s})$ is an aerodynamic transfer matrix, which determines the magnitude and phase of the aerodynamic loads generated by the airfoil motions. The term $\bar{s}$ here denotes a reduced Laplace variable, normalized by free-streem velocity U and airfoil semichord b (this is analogous to the reduced frequency parameter k often used in frequency-domain unsteady aerodynamic analysis). The reduced Laplace variable is defined as

$$\bar{s} = \frac{sb}{U} \tag{7}$$

In the frequency domain, $\boldsymbol{Q}(\bar{s})$ is readily obtained from tabulated oscillatory response data, but this frequency response data can not be directly applied to a time-domain formulation.

The frequency-domain oscillatory response data can be used to develop a time-domain unsteady aerodynamic model, however, using the rational function approximation approach. The transfer matrix $\boldsymbol{Q}(\bar{s})$ is approximated by a rational function $\tilde{\boldsymbol{Q}}(\bar{s})$, assumed to be of the form:

$$\tilde{\boldsymbol{Q}}(\bar{s}) = \boldsymbol{C}_0 + \boldsymbol{C}_1\bar{s} + \sum_{n=1}^{n_L} \frac{\bar{s}}{\bar{s}+\gamma_n}\boldsymbol{C}_{n+1} \tag{8}$$

In Eq. (8), $\boldsymbol{C}_0$ represents the quasisteady aerodynamic contribution. Because a finite response is desired as the frequency of oscillation increases, $\boldsymbol{C}_1$ is constrained to be zero. The final summation term in Eq. (8) represents n_L aerodynamic lag terms, with poles γ_n that lie on the negative real axis.

The approximate function $\tilde{\boldsymbol{Q}}(\bar{s})$ is then adjusted to achieve the best fit, in a least squares sense, to the tabulated data in $\boldsymbol{Q}(\bar{s})$ by choosing appropriate values for the elements of the matrices $\boldsymbol{C}_{n+1}$. The location of the poles γ_n are selected through an optimization process that seeks to minimize the fitting error between $\boldsymbol{Q}(\bar{s})$ and $\tilde{\boldsymbol{Q}}(\bar{s})$. This fitting process takes place in the frequency domain ($\bar{s} = i\frac{\omega b}{U} = ik$). Details of the implementation of the fitting process are provided in [19].

By choosing a rational expression for the form of the approximate model in the Laplace domain, the model can be easily transformed to the time domain. For convenience, the summation term in Eq. (8) can be rewritten using matrix notation, with the rational function taking the following form:

$$\tilde{\boldsymbol{Q}}(\bar{s}) = \boldsymbol{C}_0 + \boldsymbol{C}_1\bar{s} + \boldsymbol{D}(\boldsymbol{I}\bar{s} - \boldsymbol{R})^{-1}\boldsymbol{E}\bar{s} \tag{9}$$

where the matrices $\boldsymbol{D}$, $\boldsymbol{R}$, and $\boldsymbol{E}$ are defined as

$$\boldsymbol{D} = \begin{bmatrix} \boldsymbol{I} & \boldsymbol{I} & \cdots & \boldsymbol{I} \end{bmatrix} \tag{10}$$

$$\boldsymbol{R} = -\begin{Bmatrix} \gamma_1\boldsymbol{I} & & & \\ & \gamma_2\boldsymbol{I} & & \\ & & \ddots & \\ & & & \gamma_{n_L}\boldsymbol{I} \end{Bmatrix} \tag{11}$$

$$\boldsymbol{E} = \begin{bmatrix} \boldsymbol{C}_2 \\ \boldsymbol{C}_3 \\ \vdots \\ \boldsymbol{C}_{n_L+1} \end{bmatrix} \tag{12}$$

Substituting the rational function approximation of the aerodynamic transfer matrix in Eq. (9) into Eq. (6), and defining a vector of aerodynamic states $\boldsymbol{X}(\bar{s})$ as

$$\boldsymbol{X}(\bar{s}) = (\boldsymbol{I}\bar{s} - \boldsymbol{R})^{-1}\boldsymbol{E}\bar{s}\boldsymbol{H}(\bar{s}) \tag{13}$$

yields the following expression for the aerodynamic loads in the Laplace domain:

$$\boldsymbol{F}(\bar{s}) = \boldsymbol{C}_0\boldsymbol{H}(\bar{s}) + \boldsymbol{C}_1\bar{s}\boldsymbol{H}(\bar{s}) + \boldsymbol{D}\boldsymbol{X}(\bar{s}) \tag{14}$$

Equations (13) and (14) are then transformed from the reduced Laplace domain ($\bar{s}$) to the time domain, resulting in the following expressions:

$$\dot{\boldsymbol{X}}(t) = \frac{U}{b}\boldsymbol{R}\boldsymbol{X}(t) + \boldsymbol{E}\dot{\boldsymbol{h}}(t) \tag{15}$$

$$\boldsymbol{F}(t) = \boldsymbol{C}_0\boldsymbol{H}(t) + \boldsymbol{C}_1\frac{b}{U}\dot{\boldsymbol{H}}(t) + \boldsymbol{D}\boldsymbol{X}(t) \tag{16}$$

Equation (16) gives the aerodynamic forces and moments on a 2-D airfoil section as a function of both the generalized airfoil motions

$\boldsymbol{H}(t)$ (pitch, plunge, and flap deflection and rate) and the aerodynamic states $\boldsymbol{X}(t)$. The aerodynamic states, governed by Eq. (15), are in turn influenced by airfoil motion.

Equations (15) and (16) provide the unsteady aerodynamic loading on an airfoil section. The total aerodynamic load on the wing is determined by evaluating Eqs. (15) and (16) at several spanwise locations, then numerically integrating these sectional loads across the entire span of the wing. The unsteady airloads are added to the system equations of motion given in Eq. (4). A detailed description of the integration of the unsteady aerodynamic model with the FEM wing model is provided in [19]. For the unsteady results presented in this paper, the 2-D unsteady airloads (lift, pitching moment, and hinge moment) are evaluated at 4 spanwise locations, with 5 aerodynamic lag poles at each location ($n_L = 5$). This results in a total of 60 aerodynamic states (4 locations × 5 poles × 3 airloads–lift, pitching moment and hinge moment), which must be computed simultaneously with the system equations of motion.

Optimal Control Results

In this section, active flaperon control systems are designed to alleviate whirl flutter. Two different rotor configurations, the gimballed stiff in-plane XV-15 semispan model [23] and the hingeless soft in-plane Boeing Model 222 semispan model [2], are considered. Key model parameters are given in Table 1 for the XV-15, and in Table 2 for the Model 222. Optimal linear quadratic controllers are designed in which controller gains are selected to minimize the following quadratic cost function:

$$J = \int_0^\infty (\boldsymbol{q_A}^T[Q]\boldsymbol{q_A} + R\overset{\star\star 2}{\delta}) \, \mathrm{d}t \tag{17}$$

where $\boldsymbol{q_A}$ represents the augmented state vector in Eq. (4). If the unsteady aerodynamic model is included in the analysis, this augmented state vector also includes all of the aerodynamic lag states $\boldsymbol{X}$. The matrix $[Q]$ contains the weights placed on each state variable. It is a diagonal matrix, with the on-diagonal entries corresponding to rotor and wing displacements set to one, and all other entries [corresponding to rates, flaperon displacement, and (if present) aerodynamic lag states] set to zero. The value of the weight on control effort [the parameter R in Eq. (17)] is manually adjusted to allow the largest possible increase in flutter speed, while at the same time respecting the limits on flap actuation previously discussed. The algebraic Riccati equation is solved to determine the control gain matrix [$[G]$ in Eq. (5)] that minimizes the cost function in Eq. (17).

The optimal control results presented in this section are generated using a quasisteady aerodynamic model for the wing and flaperon aerodynamics. The effect of including unsteady aerodynamic effects will be examined in a later section.

Table 1 XV-15 full-scale test: model properties

Number of blades, N	3
Radius, R	3.81 m
Lock number, γ	3.83
Solidity, σ	0.089
Lift curve slope, $c_{l\alpha}$	5.7/rad
Rotor rotational speed, Ω	458 rpm
Pitch-gimbal coupling, K_{PG}	−0.268
Inertia properties	
I_b	142.4 kg m^2
I_β	110.9 kg m^2
$I_{\beta\alpha}$	142.4 kg m^2
I_ζ	95.45 kg m^2
$I_{\zeta\alpha}$	112.0 kg m^2
S_β	45.37 kg m
S_ζ	38.66 kg m
Blade stiffness	
$\omega_{\beta 0}$	59.8 rad/ sec
$\omega_{\zeta 0}$	103 rad/ sec
R_β	1
R_ζ	1

Table 2 Boeing 222 full-scale test: model properties

Number of blades, N	3
Radius, R	3.96 m
Lock number, γ	4.06
Solidity, σ	0.115
Lift curve slope, $c_{l\alpha}$	5.7/rad
Rotor rotational speed, Ω	386 rpm
Pitch-gimbal coupling, K_{PG}	N/A
Inertia properties	
I_b	203.4 kg m^2
I_β	187.1 kg m^2
$I_{\beta\alpha}$	193.9 kg m^2
I_ζ	174.9 kg m^2
$I_{\zeta\alpha}$	187.1 kg m^2
S_β	65.83 kg m
S_ζ	56.05 kg m
Blade Stiffness	
$\omega_{\beta 0}$	16.8 rad/ sec
$\omega_{\zeta 0}$	32.7 rad/ sec
R_β	1
R_ζ	1

XV-15

Figure 4 shows the baseline (uncontrolled) modal damping characteristics vs airspeed for the full-scale XV-15 semispan wind tunnel model, generated using a quasisteady model of wing aerodynamics. The wing vertical bending (beam) mode is the critical mode for this wing/rotor configuration, becoming unstable at 330 kn.

Performance of an optimal flaperon controller for the XV-15 is shown in Fig. 5. The optimal control system is able to improve damping for the wing modes, with wing vertical bending mode damping being particularly enhanced. The stability boundary is increased by approximately 145 kn, from 330 kn for the baseline (Fig. 4) to nearly 475 kn for the controlled system, where the rotor coning mode (β_0) reaches near-zero damping. However, the practical airspeed limit for this configuration is 420 kn, above which the required control inputs exceed the 6 deg limit imposed on flaperon deflection. This still represents a significant 90 kn increase in flutter speed over the baseline. Increasing the weight on control effort in Eq. (17) would reduce flaperon deflection, but this would also result in decreased damping augmentation in the wing modes. In particular,

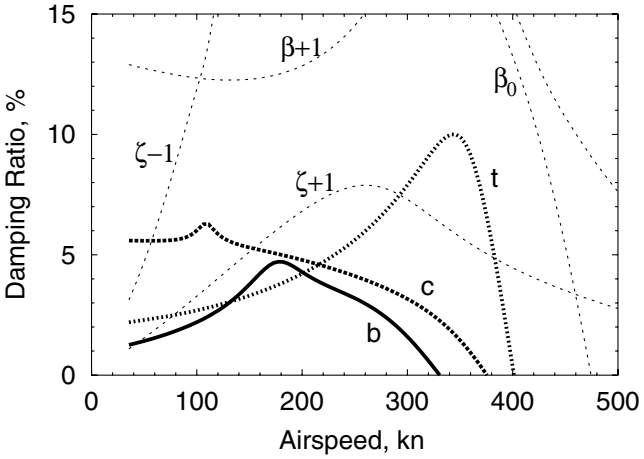

Fig. 4 XV-15: Modal damping vs airspeed for uncontrolled system [*b*: wing beam mode; *c*: wing chord mode; *t*: wing torsion mode; β_0: rotor coning mode; $\zeta - 1$, $\zeta + 1$: cyclic lag modes; $\beta + 1$: cyclic flap (gimbal) mode].

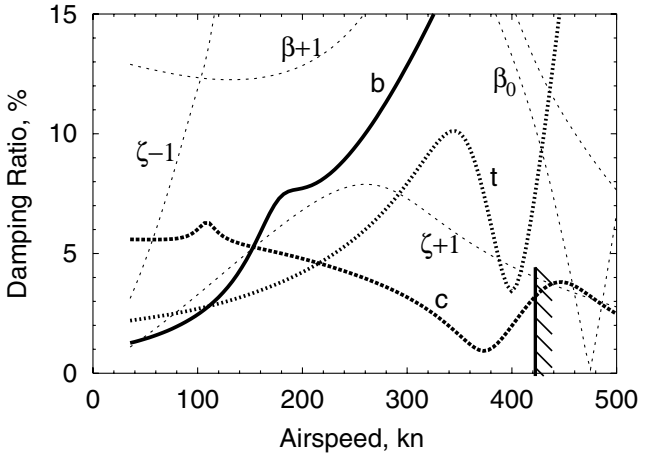

Fig. 5 XV-15: Modal damping vs airspeed with optimal wing flaperon control (flaperon deflection limit reached at 420 kn).

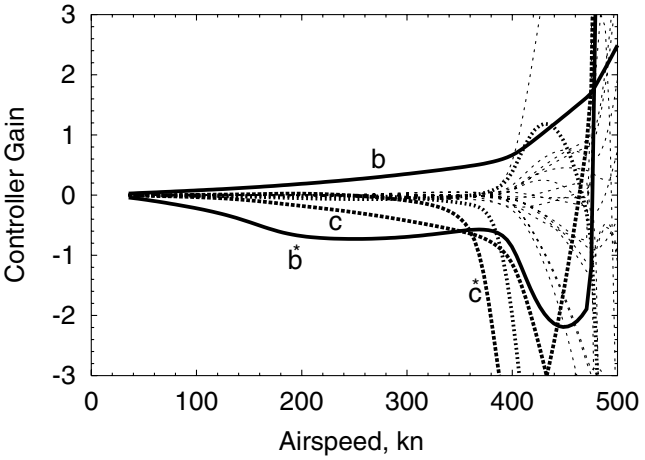

Fig. 6 XV-15: LQR optimal controller gains.

decreased damping in the wing chord mode near 380 kn would prevent safe operation above that speed.

Figure 6 shows the variation of controller gains with airspeed for the optimal flaperon control designed for the XV-15. Below about 400 kn, Fig. 6 shows that most of the feedback gains are near zero. The few nonzero gains, labeled on the figure, are on feedback of wing vertical bending mode rate ($\dot{b}$) and displacement (b), and wing chordwise bending mode rate ($\dot{c}$) and displacement (c). Of these modes, the gain on vertical bending rate feedback is the largest. Above about 400 kn, the magnitudes of the feedback gains rise sharply, due to the need for larger control inputs to provide stability. The increasingly large controller gains ultimately drive the flaperon to its deflection limit at 420 kn.

Model 222

The baseline modal damping vs airspeed behavior for the uncontrolled full-scale Model 222 wind tunnel model using quasisteady wing aerodynamics is shown in Fig. 7. For this configuration, the wing chordwise bending mode is the critical mode, whereas for the XV-15 model, the vertical bending mode was critical. The baseline Model 222 chordwise bending mode becomes unstable at 390 kn. It should be noted that the wing vertical bending mode, although not the critical mode for whirl flutter stability, does exhibit low damping levels, particularly below 200 kn.

The stability characteristics of the Model 222 with an optimal controller are shown in Fig. 8. The stability boundary is increased by about 20 kn over the baseline (Fig. 7), from 390 to just over 410 kn,

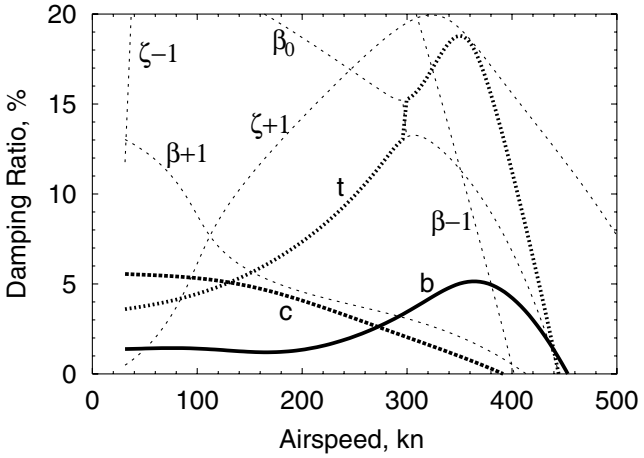

Fig. 7 Model 222: Modal damping vs airspeed for uncontrolled system (b: wing beam mode; c: wing chord mode; t: wing torsion mode; β_0: rotor coning mode, $\zeta - 1$; $\zeta + 1$: cyclic lag modes; $\beta - 1$, $\beta + 1$: cyclic flap modes).

where the rotor progressing flap mode ($\beta + 1$) reaches near-zero damping. Commanded flaperon deflections below this speed are within the imposed limits. Increasing flaperon deflection by reducing the weight on control effort in the optimal control cost function in Eq. (17) does not improve the damping of the now-critical rotor mode (unless the weight is reduced to the point that unreasonably large flaperon deflections are commanded). Besides the modest increase in flutter speed, the large increase in wing vertical bending mode damping, also seen in the XV-15, is particularly noteworthy for this configuration. The low inherent damping in the wing vertical bending mode of soft in-plane tiltrotors is significantly improved by the actively controlled flaperon.

Figure 9 shows the variation of controller gains with airspeed for the Model 222. Note that the general behavior of the gains is similar to the gains obtained for the XV-15 (compare Figs. 6 and 9). At speeds below the stability boundary, the only significant gains are those associated with feedbacks of the wing vertical and chordwise bending modes. Vertical bending mode rate feedback again has the largest gain in this speed range. At high airspeeds, the magnitude of all feedback gains begins to increase rapidly, as was the case for the XV-15.

Influence of Unsteady Aerodynamics

The results presented to this point have all been generated using a quasisteady wing aerodynamic model. The influence of unsteady

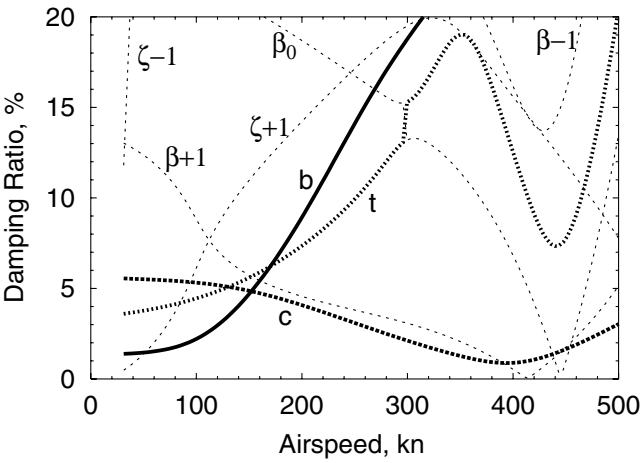

Fig. 8 Model 222: Modal damping vs airspeed with optimal wing flaperon control ($\beta + 1$ mode reaches zero damping at 412 kn).

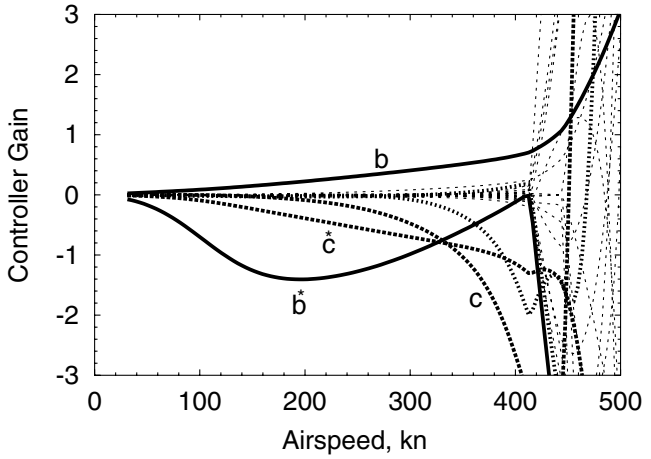

Fig. 9 Model 222: LQR optimal controller gains.

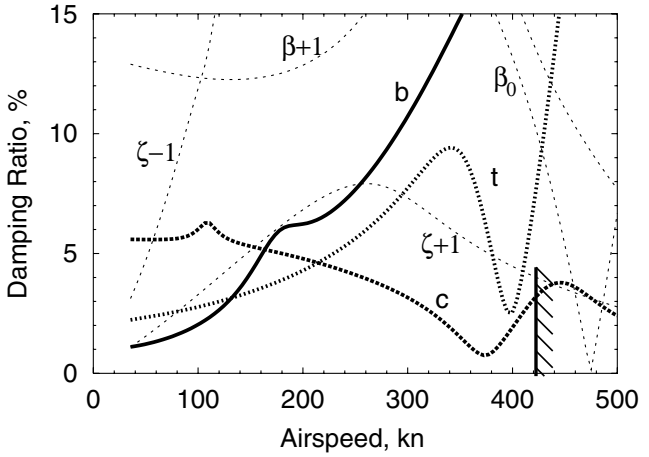

Fig. 11 XV-15: Modal damping vs airspeed with optimal wing flaperon control and unsteady aerodynamics (flaperon deflection limit reached at 420 kn).

aerodynamic effects on flaperon active control is now examined using the RFA unsteady aerodynamic model described above.

Figure 10 shows the baseline damping characteristics for the XV-15, with unsteady wing aerodynamic effects included in the analysis. Careful comparison of Fig. 10 with Fig. 4 shows only small decreases in peak damping of the wing modes when unsteady effects are included. This is consistent with observations in [24], where a Peters/He finite state wake model was applied to a tiltrotor wing. The nearly insignificant effect of wing unsteady aerodynamic effects on stability for the baseline (uncontrolled) case is due to the relatively small effect wing aerodynamic forces have on aeroelastic stability. Wing perturbation lift, drag, and pitching moments are much smaller than the perturbation forces and moments from the rotor acting on the wing.

Introducing the flaperon control system permits the controlled generation of larger wing aerodynamic forces. Nevertheless, Fig. 11 shows that including wing unsteady aerodynamic effects still results in only a slight reduction in wing damping levels achieved when flaperon active control is applied (compare with Fig. 5). The optimal control gains applied to the system in Fig. 11 are calculated while including the unsteady aerodynamic effects in the model. Figure 12 shows the variation of these controller gains with airspeed for the unsteady aerodynamics case. Though there are some differences in the values of the gains, the overall behavior of the gains is similar to the quasisteady case.

The influence of wing unsteady aerodynamics on the Model 222 is similar to that seen for the XV-15. Modal damping in the wing modes is slightly reduced for the baseline system (Fig. 13) and for the system with active flaperon control (Fig. 14). The optimal gains derived with the unsteady aerodynamics model active (Fig. 15) are similar in behavior, but not exactly the same as, the gains obtained using only quasisteady aerodynamics.

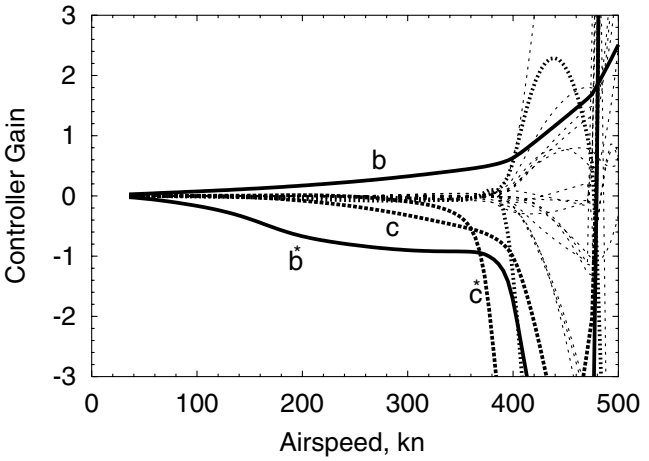

Fig. 12 XV-15: LQR optimal controller gains when unsteady aerodynamic effects are included.

The importance of including wing unsteady aerodynamics when designing flaperon control systems is further examined by looking at the stability characteristics obtained when a controller designed using the quasisteady wing aerodynamic model is run with the unsteady aerodynamics model active. Figure 16 shows the damping

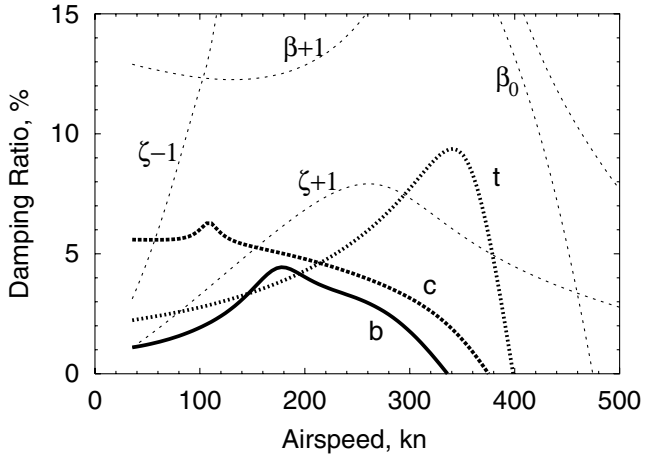

Fig. 10 XV-15: Modal damping vs airspeed for uncontrolled system, including unsteady aerodynamic model.

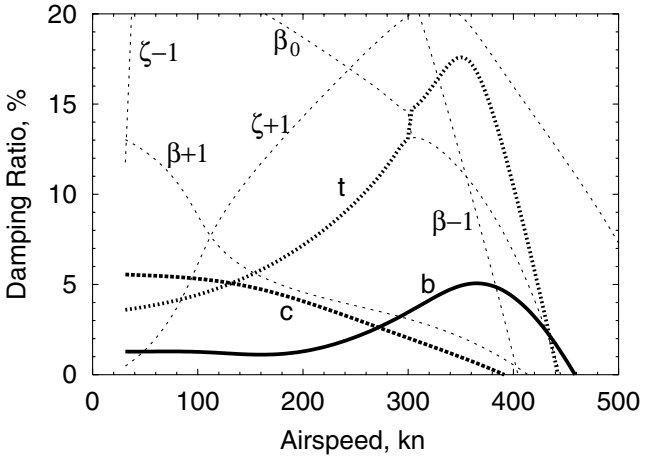

Fig. 13 Model 222: Modal damping vs airspeed for uncontrolled system, including unsteady aerodynamic model.

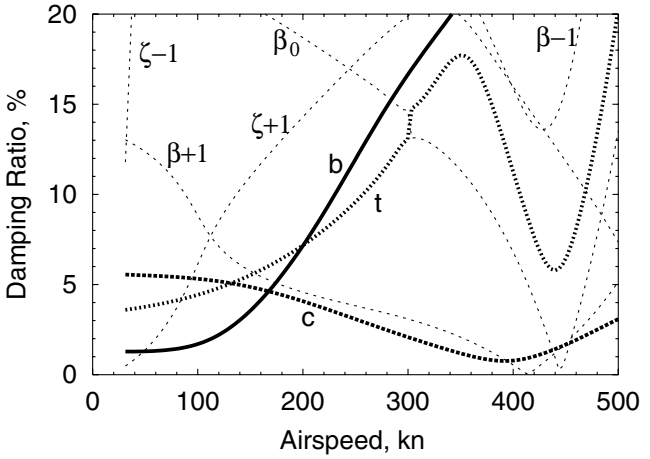

Fig. 14 Model 222: Modal damping vs airspeed with optimal wing flaperon control and unsteady aerodynamics ($\beta + 1$ mode reaches zero damping at 412 kn).

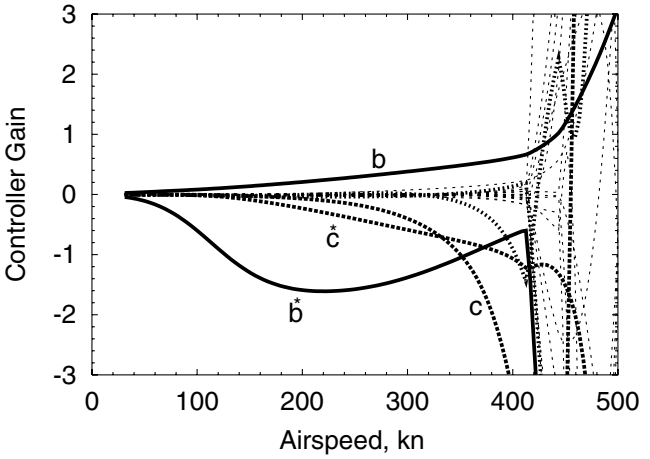

Fig. 15 Model 222: LQR optimal controller gains when unsteady aerodynamic effects are included.

characteristics in this case for the XV-15, and Fig. 17 shows the corresponding data for the Model 222. In both cases, there is a noticeable reduction in damping at high speed when compared with Figs. 11 and 14, respectively, which show damping vs airspeed when the controllers were designed with unsteady aerodynamic effects included. It should be noted that most of the differences in damping

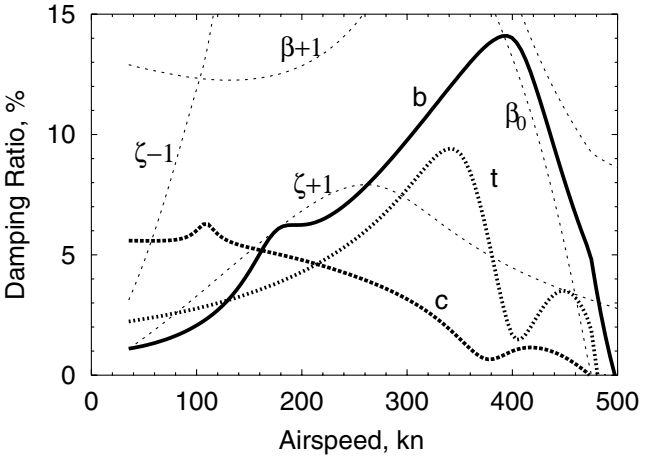

Fig. 16 XV-15: Modal damping vs airspeed for wing flaperon control with unsteady aerodynamics, controller gains obtained using quasisteady aeromodel.

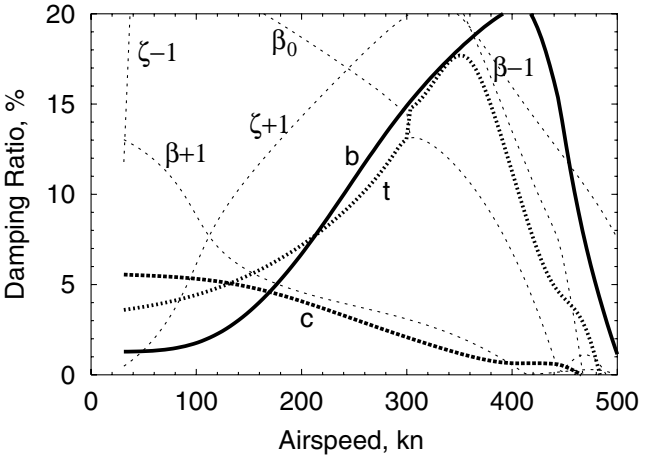

Fig. 17 Model 222: Modal damping vs airspeed for wing flaperon control with unsteady aerodynamics, controller gains obtained using quasisteady aeromodel.

observed when running with the two different sets of gains occur at airspeeds above the stability boundary, and are of no practical consequence. Because the modal damping results obtained from either aerodynamic model are similar in the airspeed range of interest, regardless of which aerodynamic model is used to design the controller, it is concluded that the simple quasisteady wing aerodynamic model is adequate to explore the basic performance of flaperon control. To obtain the greatest benefit from the flaperon control system, however, the control gains should be designed with the highest-fidelity aerodynamic model available.

Full-State Constant-Gain Controller

The optimal control results presented above featured controller gains that vary with airspeed. For each airspeed considered, a new set of gains is obtained by minimizing the cost function in Eq. (17) at that airspeed. A control system with constant controller gains is generally preferred to a more complex gain-scheduled control system. Figure 18 shows the damping characteristics of the semispan XV-15 model with a full-state constant-gain controller, using the controller gains calculated as optimal at 380 kn. Figure 19 shows the stability of the Model 222 using a constant-gain controller with the gains that were optimal at 380 kn. The data in both Figs. 18 and 19 were generated using the quasisteady aerodynamic model. For both configurations, the improvements in flutter speed and vertical bending mode damping are still maintained using the single set of control gains (as opposed to gain scheduling). Comparison of the

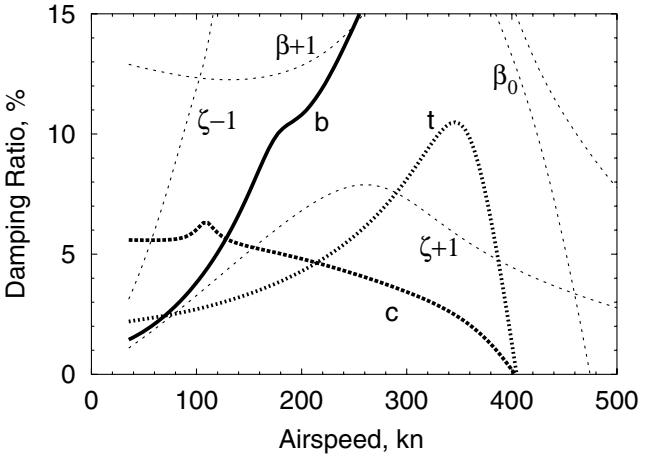

Fig. 18 XV-15: Modal damping vs airspeed for wing flaperon actuation with constant gains (optimally determined at 380 kn).

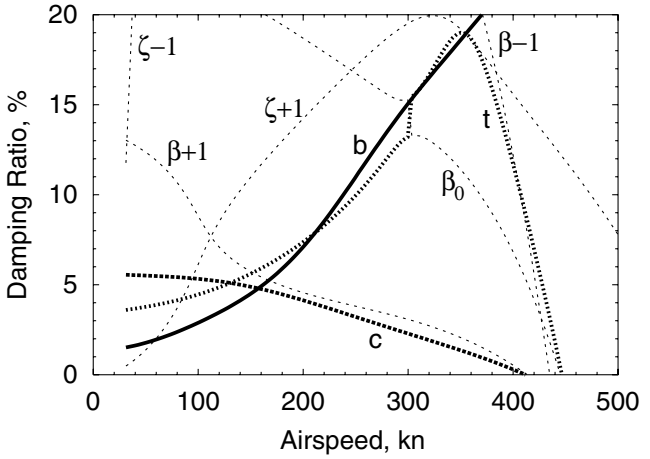

Fig. 19 Model 222: Modal damping vs airspeed for wing flaperon actuation with constant gains (optimally determined at 380 kn).

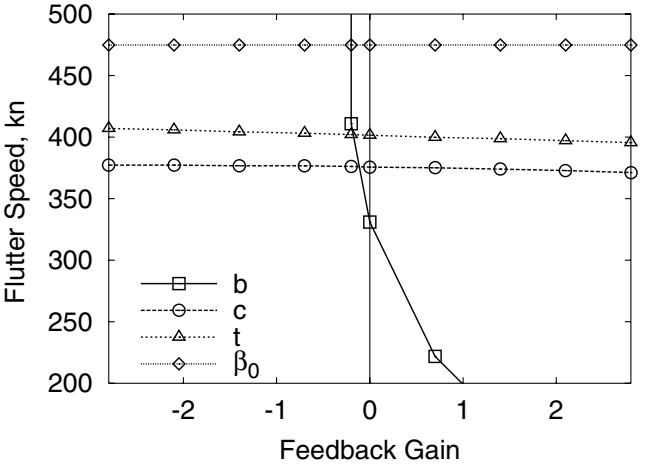

Fig. 20 XV-15: Influence of rate feedback of wing vertical bending motion on flutter speed.

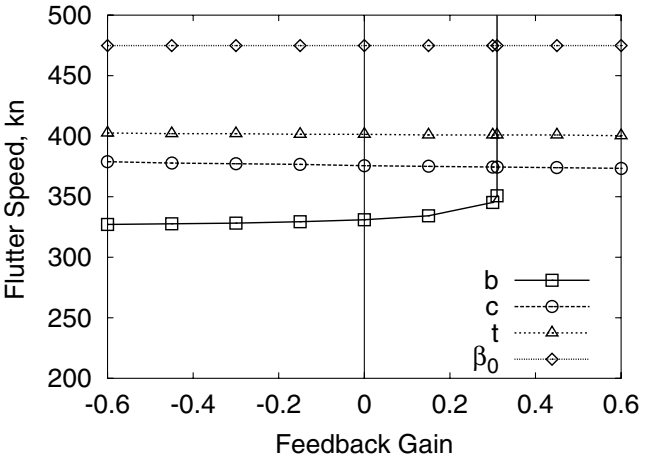

Fig. 21 XV-15: Influence of position feedback of wing vertical bending motion on flutter speed.

constant-gain results in Figs. 18 and 19 with the gain-scheduled optimal control results in Figs. 5 and 8 show that damping at speeds below the stability boundary is actually greater for the constant-gain case. This is because the control gains used at low speeds for the constant-gain case are larger than those used at those speeds by the optimal controller. As a result, flaperon actuation at low speeds is somewhat greater than for the optimally designed case. Despite the larger flaperon deflections, the constant-gain designs are still within the imposed actuation limits. To avoid the unnecessarily large flaperon deflections at low speed, the constant-gain controller could be turned off when operating at speeds where the baseline aircraft stability margins are adequate.

Investigation of Key Feedback Parameters

Examination of the controller gains obtained for both the XV-15 and Model 222 revealed that the gains on a few key feedback parameters are typically much larger than the others. Wing vertical bending and chordwise bending feedback (position and rate) dominate the optimal control solutions below the speed where controller gains rapidly increase and the flaperon reaches its deflection limits.

The influence of feedback of each of these states (vertical bending rate and position, and chordwise bending rate and position) on flutter speed is examined individually to determine the effectiveness of these parameters for use in simple output feedback control systems. Results are provided here only for the XV-15, as the Model 222 shows similar trends. The following comments and discussion apply equally to both configurations, except where noted.

Figure 20 shows the influence of wing vertical bending rate feedback on flutter speed. The figure plots the speed at which each wing mode goes unstable as a function of vertical bending rate feedback gain. The range of gains shown in the figure is limited to the range for which the resulting flaperon motion does not exceed the deflection limits. Figure 20 shows that negative vertical bending rate feedback is able to completely stabilize the wing vertical bending mode, even for very small feedback gains. The increase in vertical bending mode flutter speed is caused by a large increase in vertical bending mode damping, resulting in the mode becoming stable over the entire range of airspeeds considered. This large increase in damping is also seen in the full-state optimal control results discussed previously, and this is due to the presence of vertical bending rate feedback in the optimal control gains. The influence of feeding back vertical bending rate alone is largely restricted to this increase in vertical bending mode damping—there is little influence on the stability of the other wing modes. For the XV-15, the large increase in vertical bending mode damping produces a significant increase in critical flutter speed (about 50 kn), because the vertical bending mode is the critical flutter mode in the baseline configuration. For the Model 222, the chordwise bending mode is the critical mode, and it remains largely unaffected by feedback of vertical bending rate. However, the increased vertical bending mode damping associated with feedback of vertical bending rate is still beneficial for the Model 222, because the baseline subcritical damping (the damping at speeds below the onset of flutter) of the vertical bending mode is poor for this configuration.

As is the case for feedback of vertical bending rate, feedback of vertical bending displacement (Fig. 21) improves the flutter speed of the vertical bending mode while having relatively little influence on the other modes. Forces generated by the flaperon driven with vertical bending displacement feedback act as a negative spring on the vertical bending mode. This reduces the frequency of the vertical bending mode, and increases the frequency separation between the vertical bending and torsion modes. Increased separation of these two modal frequencies is identified in [25,26] as having a stabilizing effect on whirl flutter. Stability of the vertical bending mode is not as sensitive to displacement feedback as it is to rate feedback, however. Larger flaperon deflections are required to achieve a given level of stability augmentation when the flaperon is driven with displacement feedback. So for single-state feedback applications, vertical bending rate feedback is the preferable option.

Negative values of wing chordwise bending rate feedback gain (Fig. 22) are beneficial to chordwise bending mode stability, while at the same time reducing the stability of the vertical bending mode. The opposite trends in stability of the vertical and chordwise bending modes with chordwise bending rate feedback limit the effectiveness of this gain for independently increasing flutter speed. For the XV-15, Fig. 22 shows that a positive value of wing chordwise bending rate feedback gain can provide a modest increase in flutter speed

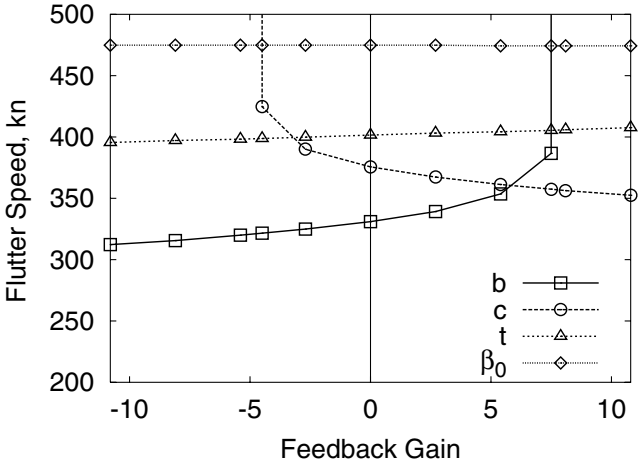

Fig. 22 XV-15: Influence of rate feedback of wing chordwise bending motion on flutter speed.

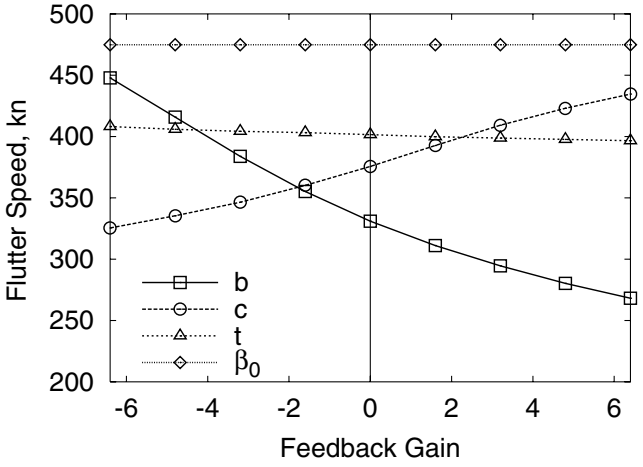

Fig. 23 XV-15: Influence of position feedback of wing chordwise bending motion on flutter speed.

(about 25 kn). For the Model 222, with the chordwise bending mode as the critical whirl flutter mode, a negative value of chordwise bending rate feedback gain is more beneficial.

Chordwise bending displacement feedback (Fig. 23) shows a similar trend to what was observed with chordwise rate feedback. In both cases, the trend of chordwise bending mode stability with gain value runs opposite to that of the vertical bending mode. So depending on which wing mode is critical for a given aircraft design, either positive or negative feedback may be the most beneficial.

The influence of any one of the feedback parameters considered here is largely limited to changing the stability of one or two modes. Depending on which mode is the critical mode for a given aircraft configuration, feedback of different states may be the most appropriate for a single-state feedback controller application. Additionally, wing vertical bending rate feedback may be attractive for any configuration, because of the large increase it provides in vertical bending mode damping at subcritical speeds. In the case of the Model 222, for example, it may be much more desirable to improve the vertical bending mode damping at moderate speed than to increase the whirl flutter speed, which at 390 kn is already much higher than that of the XV-15.

Summary and Concluding Remarks

Active control of a wing flaperon is able to improve tilt rotor whirl flutter stability margins, and can also improve the subcritical damping of wing modes. The influence of unsteady aerodynamic effects on flaperon control performance and design were investigated. Full-state constant-gain feedback control systems showed stability augmentation levels similar to the full gain-scheduled optimal controllers, at the expense of higher flaperon deflections at low to moderate speeds. Several candidate feedback parameters for simpler single-state control systems have been identified. The results of this investigation of tiltrotor whirl flutter stability augmentation using wing flaperon actuation may be summarized as follows:

1) Wing flaperon actuation has the potential to significantly increase flutter speed. The ability of the control system to increase flutter speed is ultimately dependent on details of a given aircraft configuration, such as which wing mode is the critical mode, and the stability characteristics of the rotor modes.

2) The full-state feedback optimal controller is effective for increasing stability. Below the stability boundary, the dominant gains in the optimal gain matrices are those associated with wing vertical bending and chordwise bending feedback, with wing vertical bending rate feedback having the largest gain.

3) In addition to improving whirl flutter stability boundaries for both stiff- and soft in-plane tiltrotor configurations, active control through the wing flaperon significantly increased wing vertical bending mode damping at subcritical speeds, which is particularly beneficial for soft in-plane configurations, where this mode is typically lightly damped.

4) Including unsteady wing aerodynamic effects was shown to have some influence on predicted damping levels and on optimal controller design, but did not significantly change the results when compared with simpler quasisteady aerodynamic models.

5) Optimal gains calculated at high speed provide increased damping at low speed as well, making constant-gain simplifications to the optimally designed controllers possible. The larger flap deflections at low speed associated with the constant-gain controller could be alleviated by only activating the stability augmentation at high speeds (above 300 kn, for instance).

6) Performance of a simple single-state feedback controller is limited because in general the stabilizing influence is restricted to one mode. In some cases, the simple feedback control system is still able to achieve appreciable increases in stability (as much as 50 kn). The large increases in vertical bending mode damping seen in the full-state optimal control results can also be obtained through feedback of vertical bending rate alone. For some tiltrotor configurations, a simple single-state feedback controller may provide adequate performance.

7) For tiltrotor configurations with wing modes that have closely spaced stability boundaries, a single-state feedback controller will not provide significant increases in aeroelastic stability, because the single-state feedback controller can only improve the stability of one of the two modes. As a result, the critical flutter speed will not change significantly. For such configurations, a multistate feedback control system is required.

Acknowledgment

This research was funded by the National Rotorcraft Technology Center under the Penn State Rotorcraft Center of Excellence program, with Yung Yu as technical monitor.

References

[1] Howard, A. K. T., "The Aeromechanical Stability of Soft-Inplane Tiltrotors," Ph.D. Thesis, The Pennsylvania State University, 2001.

[2] Magee, J. P., and Alexander, H. R., "Wind Tunnel Tests of a Full Scale Hingeless Prop/Rotor Designed for the Boeing Model 222 Tilt Rotor Aircraft," NASA CR 114664, Boeing Vertol Co., Oct. 1973.

[3] Nixon, M. W., Langston, C. W., Singleton, J. D., Piatak, D. J., Kvaternik, R. G., Corso, L. M., and Brown, R. K., "Aeroelastic Stability of a Four-Bladed Semi-Articulated Soft-Inplane Tiltrotor Model," *Proceedings of the 59th Annual American Helicopter Society Forum*, American Helicopter Society, Alexandria, VA, 2003.

[4] Johnson, W., "Optimal Control Alleviation of Tilting Proprotor Gust Response," *Journal of Aircraft*, Vol. 14, No. 3, March 1977, pp. 301–308.

[5] Miller, D. G., and Ham, N. D., "Active Control of Tilt-Rotor Blade In-Plane Loads During Manuevers," *Proceedings of the Fourteenth*

European Rotorcraft Forum, 1988.

[6] Settle, T. B., and Nixon, M. W., "MAVSS Control of an Active Flaperon for Tiltrotor Vibration Reduction," *Proceedings of the 53rd Annual American Helicopter Society Forum*, American Helicopter Society, Alexandria, VA, 1997.

[7] Nixon, M. W., Kvaternik, R. G., and Settle, T. B., "Tiltrotor Vibration Reduction Through Higher Harmonic Control," *Proceedings of the 53rd Annual American Helicopter Society Forum*, American Helicopter Society, Alexandria, VA, 1997.

[8] Nasu, K.-i., "Tilt-Rotor Flutter Control in Cruise Flight," NASA TM 88315, December 1986.

[9] van Aken, J. M., "Alleviation of Whirl-Flutter on Tilt-Rotor Aircraft Using Active Controls," *Proceedings of the 47th Annual American Helicopter Society Forum*, 1991.

[10] van Aken, J. M., "Alleviation of Whirl-Flutter on a Joined-Wing Tilt-Rotor Aircraft Configuration Using Active Controls," *International Specialists' Meeting on Rotorcraft Basic Research of the American Helicopter Society*, American Helicopter Society, Alexandria, VA, 1991.

[11] Vorwald, J. G., and Chopra, I., "Stabilizing Pylon Whirl Flutter on a Tilt-Rotor Aircraft," *Proceedings of the 32nd AIAA/ASME/ASCE/AHS/ASC Structures, Structural Dynamics, and Materials Conference*, AIAA, Reston, VA, 1991.

[12] Kvaternik, R. G., Piatak, D. J., Nixon, M. W., Langston, C. W., Singleton, J. D., Bennett, R. L., and Brown, R. K., "An Experimental Evaluation of Generalized Predictive Control for Tiltrotor Aeroelastic Stability Augmentation in Airplane Mode of Flight," *Proceedings of the 57th Annual American Helicopter Society Forum*, 2001.

[13] Nixon, M. W., Langston, C. W., Singleton, J. D., Piatak, D. J., Kvaternik, R. G., Corso, L. M., and Brown, R., "Aeroelastic Stability of a Soft-Inplane Gimballed Tiltrotor Model in Hover," *Proceedings of the 42nd AIAA/ASME/ASCE/AHS/ASC Structures, Structural Dynamics, and Materials Conference*, AIAA, Reston, VA, 2001.

[14] Nixon, M. W., Langston, C. W., Singleton, J. D., Piatak, D. J., Kvaternik, R. G., Corso, L. M., and Brown, R. K., "Technical Note: Hover Test of a Soft-Inplane Gimballed Tiltrotor Model," *Journal of the American Helicopter Society*, Vol. 48, No. 1, 2003, pp. 63–66.

[15] Kvaternik, R. G., "Exploratory Studies in Generalized Predictive Control for Active Aeroelastic Control of Tiltrotor Aircraft," NASA TM-2000-210552, 2000.

[16] Hathaway, E. L., and Gandhi, F., "Modeling Refinements in Simple Tiltrotor Whirl Flutter Analyses," *Journal of the American Helicopter Society*, Vol. 48, No. 3, July 2003, pp. 186–198.

[17] Hathaway, E., and Gandhi, F., "Design Optimization for Improved Tiltrotor Whirl Flutter Stability," *Proceedings of the 29th European Rotorcraft Forum*, 2003.

[18] Theodorsen, T., "General Theory of Aerodynamic Instability and the Mechanism of Flutter," NACA Report No. 496, 1935.

[19] Hathaway, E. L., "Active and Passive Techniques for Tiltrotor Aeroelastic Stability Augmentation," Ph.D. Thesis, The Pennsylvania State University, 2005.

[20] Maisel, M., "Tilt Rotor Research Aircraft Familiarization Document," NASA TM X-62,407, Jan. 1975.

[21] Piatak, D. J., Kvaternik, R. G., Nixon, M. W., Langston, C. W., Singleton, J. D., Bennett, R. L., and Brown, R. K., "A Parametric Investigation of Whirl-Flutter Stability on the WRATS Tiltrotor Model," *Journal of the American Helicopter Society*, Vol. 47, No. 2, 2002, pp. 134–144.

[22] Myrtle, T. F., "Development of an Improved Aeroelastic Model for the Investigation of Vibration Reduction in Helicopter Rotors Using Trailing Edge Flaps," Ph.D. Thesis, University of California, Los Angeles, 1998.

[23] Anon, "Advancement of Proprotor Technology Task II: Wind-Tunnel Test Results," NASA CR 114363, Bell Helicopter Co., Sept. 1971.

[24] Stettner, M., Schrage, D. P., and Peters, D. A., "Application of a State-Space Wake Model to Tiltrotor Wing Unsteady Aerodynamics," *Proceedings of the American Helicopter Society Aeromechanics Specialists Conference*, American Helicopter Society, Alexandria, VA, 1994.

[25] Gaffey, T. M., Yen, J. G., and Kvaternik, R. G., "Analysis and Model Tests of the Proprotor Dynamics of a Tilt-Proprotor VTOL Aircraft," *Proceedings of the Air Force V/STOL Technology and Planning Conference*, 1969.

[26] Nixon, M. W., "Aeroelastic Response and Stability of Tiltrotors with Elastically-Coupled Composite Rotor Blades," Ph.D. Thesis, University of Maryland, 1993.

E. Livne
Associate Editor